Lightweight geopolymer-based hybrid materials

CrossMark

Giuseppina Roviello [a, b, *], Costantino Menna [c], Oreste Tarallo [d], Laura Ricciotti [c], Francesco Messina [a, b], Claudio Ferone [a, b], Domenico Asprone [c], Raffaele Cioffi [a, b]

[a] Dipartimento di Ingegneria, Università di Napoli 'Parthenope', Centro Direzionale, Isola C4, 80143 Napoli, Italy
[b] INSTM Research Group Napoli Parthenope, National Consortium for Science and Technology of Materials, Via G. Giusti, 9, 50121 Firenze, Italy
[c] Dipartimento di Strutture per l'Ingegneria e l'Architettura, Università di Napoli Federico II, Napoli 80125, Italy
[d] Dipartimento di Scienze Chimiche, Università Degli Studi di Napoli "Federico II", Complesso Universitario di Monte S. Angelo, Via Cintia, 80126 Napoli, Italy

ARTICLE INFO

ABSTRACT

The present study reports on the preparation and characterization of new organic-inorganic geopolymer based hybrid foams obtained by reacting an aluminosilicate source and an alkalisilicate solution with mixtures of dialkylsiloxane oligomers or organic resins precursors. By using different amounts of Si^0 powder as *in situ* foaming agent, hybrid geopolymer-based foams with densities ranging from 0.25 to 0.85 g/cm^3 were successfully prepared. These new materials are characterized by remarkable mechanical properties, good fire resistance and low thermal conductivity, significantly better than those shown by neat geopolymer foams reported in the literature and comparable or even better than those of typical (not geopolymer) inorganic foamed materials with similar densities.

© 2017 Elsevier Ltd. All rights reserved.

1. Introduction

Porous materials are widely used in several applications including membranes, high-efficiency adsorption materials, catalysis, as well as in the construction industry where they find their application as insulating or sound-proof panels or for the production of lightweight structural components. To these aims, organic polymers, metals or inorganic materials can be successfully used as source raw material for the foamed products. In particular, thanks to their low mass, low heat conductivity and good sound-proofing properties, organic polymer foams are particularly suitable as insulating components and are extensively used in civil engineering. However, most polymeric systems suffer from thermal degradation under high temperatures, affecting their structural integrity and releasing toxic or flammable gases into the atmosphere.

In the case of high temperature applications, as an alternative to polymeric foams, inorganic porous materials can be used. Such materials are usually divided in two main classes, relying on the specific use. One class comprises materials obtained by employing lightweight aggregates while the other one is represented by highly porous materials. Several studies have been carried out about lightweight and eco-compatible materials/aggregates [1–5] employing cold bonding techniques but the obtained densities (even less than 2000 kg/m^3 defining lightweight aggregates) are, however, still considerable. Slightly lower values have been obtained by employing thermal processes [6] but such processes typically imply a high environmental impact (production of CO_2). Among inorganic porous materials, great attention has been devoted to porous geopolymers due to i) the possibility of using low cost raw materials [7,8], ii) their chemical resistance [9], iii) their good thermal properties [10] and iv) their environmental friendly nature [11,12].

The term "geopolymer" was originally introduced by Davidovits [13] to describe the amorphous inorganic aluminosilicate framework produced by reacting natural Si- and Al-rich materials, such as metakaolin or industrial by-products (fly ash, blast furnace slag), with highly alkaline aqueous solutions. Geopolymers exhibit a wide variety of technologically relevant properties, such as high compressive strength [14], fire resistance and low shrinkage [15]. For these reasons, geopolymers seem to be a desirable alternative to ordinary Portland cement also thanks to their environmentally sustainable characteristics [16] mainly associated with the reduced CO_2 emissions arising from the production of the raw materials from which they are obtained [17].

Geopolymers are produced by means of a polycondensation reaction (the so called "geopolymerization"). During this reaction, a gel network is formed, consisting of SiO_4 and AlO_4 tetrahedra

---

sharing oxygen corners and forming rings of various sizes analogous to those found in zeolites. If foaming agents are added into the geopolymer paste during its consolidation, porous materials can be obtained. Well know blowing agents are hydrogen peroxide, metallic Al or Si powder [18–20]. By following this synthesis approach, porous materials with pore size ranging from nanometers to few millimetres and a total porosity up to 90% were obtained [21,22] without using high temperature treatments (such as burn out of organics and sintering) that are, by contrast, necessary for the production of porous ceramics through conventional techniques [23].

In general, the geopolymer-based porous materials developed to date exhibit very interesting properties in terms of thermal and acoustic conductivity but the presence of pores and the extremely heterogeneous structure affect unavoidably their mechanical properties, sometimes resulting in low compressive strengths (found to be about 1 MPa or less depending on the corresponding apparent density) [20]. In detail, consolidated foams characterized by thermal conductivity values of approximately 0.15 $Wm^{-1}K^{-1}$ or less were successfully obtained with the addition of silica fume or silicon powder [21] as a foaming agent to sodium silicate and kaolin [24] or potassium silicate based [25] geopolymers. In the cited studies, the authors exploited the capability of free silicon contained inside the silica fume to generate porosity by releasing molecular hydrogen from silicon oxidization in alkaline solution, achieving significant percentages of pore volume (>60%) [26]. Porous geopolymer materials were also produced starting from fly ash precursors and in combination with hydrogen peroxide [27] or sodium perborate [28] as foaming agent, resulting in consolidated foams with a porosity of ≈80%, thermal conductivity of ≈0.08 $Wm^{-1}K^{-1}$ and compressive strengths ranging between 0.80 and 0.40 MPa. Higher compressive strengths were recorded in the case of fly ash based geopolymer foams with bulk densities in the range of 400–800 kg/m^3 and obtained with the use of aluminium powder as blowing agent [29]. Furthermore, in the case of geopolymer and fly ash foam concretes, the higher densities of the obtained materials (typically from 720 to 1600 kg/m^3) led to very high compressive strengths ranging from 3 to 48 MPa, with thermal conductivity values in the range of 0.15–0.48 $Wm^{-1}K^{-1}$ [30] which are reasonably low for concrete applications.

Recently we succeeded in obtaining organic-inorganic hybrid materials by reacting an aluminosilicate source and an aqueous alkali hydroxide and/or alkalisilicate solution with mixtures of dialkylsiloxane oligomers or organic resins precursors [31–38]. Compared to neat geopolymers with analogous Si/Al ratio, these materials are characterized by enhanced mechanical properties, along with good temperature and fire resistance [39–42].

In this study, for the first time, we report on the synthesis and characterization of high performance organic-inorganic hybrid foams obtained by *in situ* foaming of the hybrid materials described before through the addition of silicon powder. These foams show remarkable mechanical properties, good fire resistance and low thermal conductivity, significantly enhanced in respect to those characterizing neat geopolymer foams reported in the literature and comparable, or even better, than those of typical (not geopolymeric) inorganic foamed materials with similar densities.

Considering that commonly used organic insulating materials are flammable while inorganic ones need complex processing conditions and/or high sintering temperatures (increasing the manufacturing cost), the hybrid porous geopolymer-based materials described in this study have good application potential as an effective alternative for thermal insulation or fire-resistant sealant materials.

2. Experimental section

2.1. Materials

Metakaolin was kindly provided by Neuchem S.r.l. (Milan, Italy) and its composition is reported in Table 1. Sodium hydroxide with reagent grade, was supplied by Sigma-Aldrich. The sodium silicate solution was supplied by Prochin Italia S.r.l (Caserta, Italy). with the composition reported in Table 1. A commercial oligomeric dimethylsiloxane mixture was purchased from Globalchimica S.r.l (Turin, Italy) with the name of Globasil AL20. The epoxy resin used in this paper, called Epojet®, was purchased by Mapei S.p.A (Milan, Italy) [43]: it is a commercial two-component epoxy adhesive for injection, which, after the mixing, takes the aspect of a low viscosity liquid and it is usable for 40 min at room temperature. Silicon powder ~325 mesh was purchased from Sigma-Aldrich. Additional experimental details are reported in references 32 and 33.

2.2. Specimen preparation

2.2.1. Geopolymer (G-MK)

The alkaline activating solution was prepared by dissolving solid sodium hydroxide into the sodium silicate solution. The solution was then allowed to equilibrate and cool for 24 h. The composition of the solution can be expressed as Na_2O $1.4SiO_2$ $10.5H_2O$. Metakaolin was then incorporated into the activating solution with a liquid to solid ratio of 1.4:1 by weight, and mixed by a mechanical mixer for 10 min at 800 rpm. As revealed by EDS analysis on the cured samples, the composition of the whole geopolymeric system can be expressed as Al_2O_3 $3.5SiO_2$ $1.0Na_2O$ $10.5H_2O$, corresponding to a complete geopolymerization process. Neat geopolymer sample was indicated as G-MK.

2.2.2. Foamed geopolymer composites (G-Ep)

Geopolymer-based foamed composites were obtained by adding 10% by weight of Epojet® resin to the freshly-prepared geopolymeric suspension, and quickly incorporated by controlled mixing (5 min at 1350 rpm) [32]. Before being added to the geopolymeric mixture, Epojet® was cured at room temperature for 10 min, when it was still easily workable and long before its complete crosslinking and hardening (that takes place in about 5–7 h at 23 °C).

In order to obtain a smooth but effective foaming process, silicon powder was then added as foaming agent with different wt% ratios, ranging between 0.03 and 0.24%; afterwards, the system was mixed for further 5 min at 1000 rpm. The consolidated geopolymer/ organic resin samples obtained through the above mentioned procedure are hereafter indicated as G-EpXX, where XX refers to the decimal units by weight (percentage) of silicon foaming agent added to the geopolymer composite paste (e.g. G-Ep03 refers to a Geopolymer-Epojet composite with 0.03% by weight of Si content; G-Ep12 corresponds to 0.12% wt% of Si content). The composite

Table 1
Chemical composition (weight %) of the metakaolin and sodium silicate solution used in this paper.

Metakaolin							
Al_2O_3	SiO_2	K_2O	Fe_2O_3	TiO_2	MgO	CaO	others
41.90	52.90	0.77	1.60	1.80	0.19	0.17	0.67

Sodium silicate solution		
SiO_2	Na_2O	H_2O
27.40	8.15	64.45

sample that did not undergo the foaming process was indicated as G-Ep. The mix design details of G-Ep specimens are reported in Table 2.

2.2.3. Foamed geopolymer hybrids (G-Sil)

Hybrid polysiloxane-geopolymer foamed samples were prepared by incorporating 10% by weight of a commercial oligomeric dimethylsiloxane mixture into the freshly prepared geopolymeric suspension under mechanical stirring, when the polycondensation reaction of both geopolymer and dimethylsiloxane were already started but far to be completed. In order to obtain a set of samples with a different degree of porosity, silicon powder was added to the geopolymer-hybrid suspension as foaming agent in different wt% ratios, ranging between 0.03 and 0.24%; then, the system was mixed for further 5 min at 1000 rpm. These samples are hereafter indicated as G-SilXX, where XX refers to the decimal units by weight (percentage) of silicon foaming agent added to the geopolymer paste (e.g. G-Sil03 refers to a polysiloxane-geopolymer hybrid sample with 0.03% by weight of Si content while G-Sil12 corresponds to 0.12% wt% of Si content). The hybrid sample that did not undergo the foaming process was indicated as G-Sil. The mix design details of G-Sil specimens are reported in Table 2.

2.2.4. Curing treatments

As soon as prepared, all the specimens were casted in cubic molds and cured in >95% relative humidity conditions at room temperature (≈ 22 °C) for 24 h and then at 60 C for further 24 h. Subsequently, the specimens were kept at room temperature for further 5 days in >95% relative humidity conditions and then for further 21 days in air.

2.3. Methods

2.3.1. Physical testing and microstructure

SEM analysis was carried out by means of a Nova NanoSem 450 FEI Microscope.

Hydrostatic weighing for apparent density and open porosity measurements was carried out by means of a balance OHAUS-PA213 provided by Pioneer.

Average pores diameter was determined by optical image analysis of polished surfaces. The analysis was performed by means of an in-house routine developed using a commercial software package (Matlab R2015a) [44].

2.3.2. Rheological measurement

Simple flow measurements related to pastes can be performed by means of the minislump cone test [36]. This testing technique represents a simple procedure that is employed quite frequently in literature since it allows making both qualitative and quantitative observations on fresh slurries. However, the geometry of the experimental setup is not standardized and varies in a wide range [45–49]. In this work, the geometry of the minislump cone was had the following dimensions: top diameter equal to 5.0 cm; bottom diameter equal to 6.8 cm; height equal to 6.5 cm (corresponding to a paste volume equal to 179.1 cm^3). Freshly prepared slurries were slowly poured in the cone placed on a horizontal plane and carefully compacted by means of a thin steel rod. Slump orthogonal diameters were measured and the average diameter was used to calculate minislump area. Mini-slump measurements were repeated at 0, 15, 30, 60 and 120 min in order to enlighten workability loss depending on time, by keeping the fresh slurries in controlled environment (T = 20 ± 2 °C; sealed container). Apparent viscosity of geopolymeric mixtures was assessed by means of a Brookfield viscometer DV2T. Test were carried out with different spindles considering the variation of rheological features of investigated mixtures. Spindles used are standardized for the indicated device and are indicated by numbers, namely n° 4, 5, 6 and 7.

Additional tests were carried out in order to understand the capability of geopolymer slurries to retain liquid phase. Hence, washout tests were performed by means of a modified experimental setup with respect to the one used in literature [50]. In particular, instead of 750 mL beakers, 500 mL ones were used. Washout loss after dilution in distilled water was expressed in percentage compared to the initial mass.

2.3.3. Mechanical testing

Uniaxial compression tests were carried out according to of ASTM D 1621 on $50 \times 50 \times 50$ mm cubic specimens by using a MTS 810 servo-hydraulic universal testing machine. For each sample type, three specimens were tested under displacement control in order to obtain the corresponding stress-strain curve, compressive strength and Young's modulus. Compression tests were performed until the sample densified and/or ruptured at a constant displacement velocity of 0.60 mm/min. The measurement of the displacement was performed through the crosshead displacement while the Young's modulus of each sample was computed from the initial linear stress-strain response recorded during the test. All values presented in the current work are an average of three samples.

Table 2
Mix composition (wt%), apparent density and open porosity of the studied samples.

Sample	MK	SS	NaOH	Epoxy Resin	DMS	Si	Open porosity (%)	Apparent density (g cm^{-3})
G-MK	41.55	50	8.45				15%	1.524
G-Ep	37.4	45.0	7.6	10			22%	1.425
G-Ep03	37.4	45.0	7.6	10	–	0.03	38%	0.860
G-Ep06	37.4	45.0	7.6	10	–	0.06	41%	0.629
G-Ep12	37.4	45.0	7.6	10	–	0.12	48%	0.500
G-Ep14	37.4	45.0	7.6	10	–	0.14	49%	0.431
G-Ep18	37.4	45.0	7.6	10	–	0.18	50%	0.363
G-Ep24	37.4	45.0	7.6	10	–	0.24	52%	0.312
G-Sil	37.4	45.0	7.6	–	10		7%	1.339
G-Sil03	37.4	45.0	7.6	–	10	0.03	27%	0.701
G-Sil06	37.4	45.0	7.6	–	10	0.06	41%	0.508
G-Sil12	37.4	45.0	7.6	–	10	0.12	46%	0.396
G-Sil14	37.4	45.0	7.6	–	10	0.14	54%%	0.365
G-Sil18	37.4	45.0	7.6	–	10	0.18	60%	0.320
GSil24	37.4	45.0	7.6	–	10	0.24	75%	0.252

MK = metakaolin; SS = sodium silicate solution; epoxy resin = Epojet® resin; DMS = oligomeric dimethylsiloxane mixture; Si = silicon powder.

2.3.4. Thermal characterization

The thermal conductivity measurement was performed in accordance with UNI EN 1745 and UNI EN 12664, by means of the Guarded Hot Plate Method on air-dry samples with conditioning at 50 °C. The measurement equipment used follows ASTM E1530. For each sample examined, three specimens with diameter 50.8 ± 0.3 mm and thick 4.3 mm at 10 °C were tested.

The test specimens were installed between heating and cooling plates. A constant heat flow flowed through the test specimens in the stationary temperature state. Thermal conductivity was determined by the heat flow and the temperature difference between the sample surfaces. The calibration was performed on a series of reference samples with certified thermal characteristics. The thermal conductivity λ (W/mK) can be determined according to the following:

$$R_s = \frac{s}{\lambda} \tag{1}$$

where s is the specimen thickness and R_s is the thermal resistance.

2.3.5. Fire testing

Flame tests were performed by a cone calorimeter in accordance with the procedure described in ISO5660 standard method. The heat flux produced was 50 kW/m^2 on the specimen, which had an exposed surface of 100×100 mm. The testing equipment consisted of a radiant electric heater in trunk-conic shape, an exhaust gas system with oxygen monitoring and instrumentation to measure the gas flux, an electric spark for ignition, and a load cell to measure the weight loss. The test was terminated after 600 s of exposure.

3. Results and discussion

3.1. Foaming process

As described in the previous section, different amounts of silicon powder were added as foaming agent to the neat geopolymer slurry (G-MK) and to the two hybrid organic-geopolymer systems G-Ep and G-Sil. As far as G-MK slurry is concerned, due to its very low viscosity (see section 3.2), the foaming process yielded the rapid collapse of the foamed structure initially formed. For this reason, foamed G-MK samples were not considered in this discussion. On the contrary, the addition of the foaming agent to G-Ep and to G-Sil slurries produced homogeneously foamed structures. Volume expansion and density of the different G-Ep and G-Sil foamed samples obtained are reported in Fig. 1.

As expected, the effectiveness of the foaming process was strictly dependent on the Si amount added to the G-Ep and G-Sil slurry as foaming agent. The volume expansion of the not cured slurry increases with increasing the amount of the foaming agent while the density of the cured porous materials decreases as the amount of foaming agent used increases. For silicon amount ranging from 0.03% to 0.24 wt%, high resolution optical photographs of the specimens after expansion and curing, are reported in Fig. 2.

By examining the morphologies shown in Fig. 2, it is clearly apparent that macropores are observable in all samples and, for each composition, they are rather uniformly distributed in the specimens, resulting in good homogeneity also in terms of dimension and shape. Only a minor amount of egg-shaped pores was detected, parallel to the expansion direction, probably attributable to the shape and dimensions of the used mold.

As expected, a low quantity of silicon powder added as foaming agent led to poorly expanded structures with small and regularly distributed rounded pores while high Si content produced the coalescence of the pores. Average diameters of pores were equal to 0.70, 1.33, 2.28 and 4.84 mm for G-Sil03, G-Sil06, G-Sil12 and G-Sil24, respectively while were equal to 0.57, 0.85, 1.28 and 3.13 for G-Ep03, G-Ep06, G-Ep12 and G-Ep24, respectively. Although not reported in this study, it's worth pointing out that the addition of Si in amounts of more than 0.24 wt% caused the unstable collapse of the foamed microstructure. The morphological characterization is very useful to receive information about the micromechanical model [51–53].

By examining the morphologies of the foams by SEM micrographs (Fig. 3), it is worth pointing out that, as expected, the surfaces of both samples appeared to be very different from the typical microstructure of an unfoamed geopolymer matrix [32,33]. In particular, in the case of G-Ep series of samples, a 3D pore structure was detected and characterized by interconnected channels passing throughout the specimen. In the case of G-Sil foams, the microstructure was characterized by isolated pores uniformly distributed within the specimens, showing good homogeneity, also in terms of dimensions and shape. This different morphology was rationalized in terms of rheological properties of the two slurries (next paragraph).

As discussed in paragraph 3.4, these different microstructures of the two sets of samples turned out in different mechanical behaviours.

3.2. Rheology

Slump test results are reported in Fig. 4 and refer to the G-MK, G-Sil and G-Ep slurries tested as soon as prepared and for different resting times. The system exhibiting the largest flow is G-MK, while an intermediate performance was obtained for G-Sil. At variance, G-Ep was able to keep almost unchanged the shape of the slump cone after cone lifting due to very high values of viscosity and yield stress, thus indicating a strongly different rheological performance respect other investigated materials. In terms of workability loss, the two "flowable" systems, i.e. G-MK and G-SIL, exhibited a similar behaviour. Particularly, the system G-MK was able to keep its characteristic flow area for at least 30 min; this represents a significant parameter for most of the technological processing procedures on laboratory and industrial scale. G-Sil exhibited a faster workability loss with respect to G-MK, since after flow measured after 30 min was about 10% of initial slump value. G-Ep did not experience any significant change over time since the starting value of mini slump area, which was substantially similar to the bottom area of the cone, was kept almost constant for all subsequent measurements.

Apparent viscosity measurements related to G-MK, G-Sil and G-Ep slurries are reported in Fig. 5. Measurements were performed with different rotating spindles in order to provide further information and ensure a better reproducibility of the results. The possibility of using several spindles depends on the viscosity of the investigated suspension: for relatively high viscosity values, the number of suitable spindles is limited. In Fig. 5, it is evident that G-Sil is characterized by higher viscosity than G-MK since the number of suitable spindles (spindle n°5 and spindle n°6) is limited with respect to those that are suitable for G-MK (spindles n°4, n°5 and n°6). In the torque range investigated, the two mixtures exhibited a very different rheological behaviour. First, for G-MK, a plateau of apparent viscosity was clearly detected, while for G-Sil, a slight decrease was detected as a function of torque growth.

With regard to the apparent viscosity related to G-Ep slurry, it must be pointed out that measurement was strongly influenced by the applied shear regime. Hence, a significant variation of apparent viscosity was experienced depending on different torque applied. In the same range of investigated torque for other systems, G-Ep
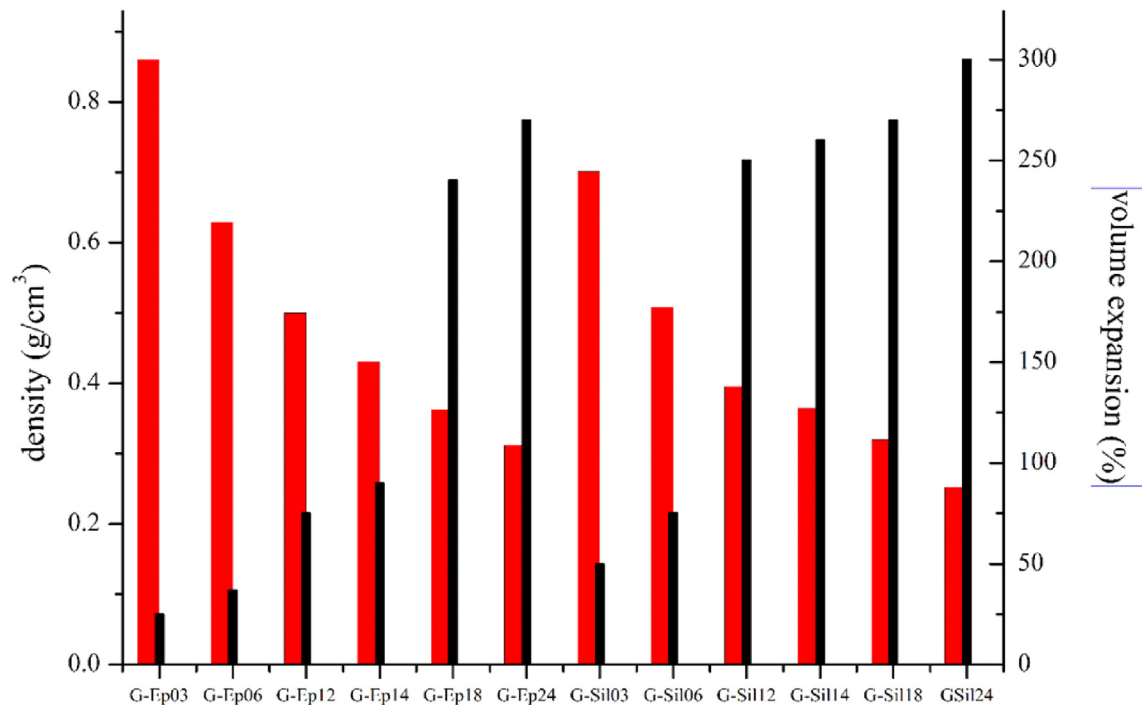
Fig. 1. Density values (red bars) and volume expansion (black bars) of G-Ep and G-Sil foamed samples. Volume expansion was evaluated by the percentage ratio between the volume of the specimen after the foaming process and the starting volume of the slurry. (For interpretation of the references to colour in this figure legend, the reader is referred to the web version of this article.)

slurry exhibited an apparent viscosity equal to $6.8 \cdot 10^5 \pm 0.4 \cdot 10^5$ cP. The presence of a plateau viscosity value was shifted at higher torque (torque > 80%). The apparent viscosity values are evidently much higher than in the other cases corresponding to G-MK and G-Sil slurries. This fact corresponds also to the restrained choice in terms of suitable spindles, which was limited only to spindle n°7.

Finally, Fig. 6 shows washout loss values for the three investigated slurries: for all the systems, a highly promising water retention capability was detected thus indicating a good processability of the material before its hardening.

The different rheological behaviours herein discussed allowed for a possible interpretation of the different foaming performances observe for the three investigated systems. Actually, we can infer that the neat geopolymer prepared in this study was not able to develop a properly foamed microstructure, due to the very low viscosity of the slurry. The addition of silicone or epoxy resin to the geopolymer slurry turned out in a significant increase of the viscosity of the system that allows the development of stable pores, thus resulting in a properly foamed microstructure. Moreover, the different rheological behaviour of the G-Sil and G-Ep systems is probably connected with the different microstructure of the two samples [32,33]. In fact, G-Ep is a geopolymer based composite system containing discrete microspheres of epoxy resin (mean diameter 10–20 μm), homogenously dispersed in the geopolymer matrix (see Fig. 3B). At variance, G-Sil is a hybrid geopolymer material obtained through the chemical bonding between silicon atoms of the geopolymer structure with the silicon atoms of the dimethylsiloxane oligomer moieties, characterized by a single phase, with compact and continuous microstructure, up to nanometric level (see Fig. 3D) [32,33].

3.3. Physical and mechanical properties

Physical and mechanical properties of foamed hybrid and composite geopolymers are herein discussed in terms of material apparent density and uniaxial compressive behaviour, including compressive strength and Young's modulus results.

The average apparent densities of G-Sil (blue symbols) and G-Ep (red symbols) foams are reported in Fig. 7 as a function of the wt% of Si powder added to the geopolymer slurry during foaming procedure. The two foamed materials exhibited a decrease of bulk density with increasing the Si content in the range 0.03–0.24 wt%, following a 2nd order polynomial law. The obtained trends suggested that lower densities were achieved as a consequence of the coalescence of individual cells of roughly constant smaller pore size (see Figs. 2 and 3) into large voids. However, G-Sil foamed material was able to reach lower density values than G-Ep foamed material when using an equal content of foaming agent. In particular, G-Sil foamed material exhibited an average apparent density varying between 0.25 and 0.70 g/cm^3 whereas, in the case of G-Ep foamed material, the density values varied between 0.31 and 0.86 g/cm^3. In other words, within the density range obtained with the same amount of foaming agent, G-Sil foam was averagely less dense by 20%. This feature is mainly related to the rheological proprieties of the two different initial materials which affected cell nucleation, growth and coarsening mechanisms taking place during the foaming process. Indeed, as reported in the previous section, the G-Ep system was characterized by very high values of viscosity and yield stress. During the expansion process, the gas volume in the growing cell increases driven by the gas pressure generating inside the cell itself, until the pressure inside the cell equals to its surrounding pressure, which is a function of surface tension and viscosity of the fresh matrix material. Because of greater viscosity of G-Ep material, a lower surface area is required to make the cell in equilibrium with its surrounding matrix which turns in smaller cell sizes of the foamed material (Fig. 2). Furthermore, the dense spheres of epoxy resin forming the heterogeneous microstructure of G-Ep system may have acted as physical obstacle for cell growth
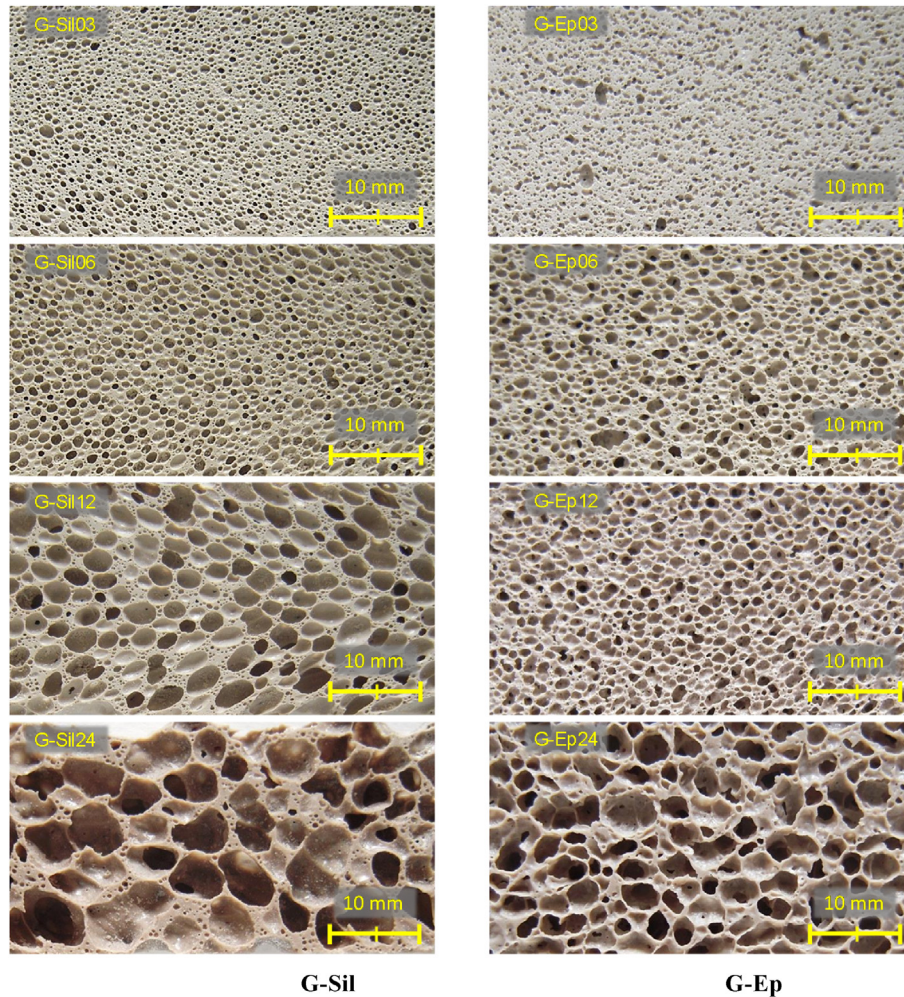
Fig. 2. Optical images of polished section surfaces of some representative G-Sil (left column) and G-Ep (right column) specimens.

phase. On the contrary, in the case of G-Sil material, the lower viscosity of the system allowed for a larger volume growth, which led to a decrease of the stability of the foam, causing, in turn, individual cells to coalesce producing larger voids (Fig. 2).

Because of the large number of specimens tested, only the stress-strain curves of the samples that revealed a representative mechanical performance were reported in Fig. 8. The stress–strain curves for each tested foam type were found to be similar kind. In details, all the investigated foamed materials exhibited a well defined elastic regime, which was noticeable at the early stages of stress (stage 1). The linear elastic regime remained with an almost constant slope until reaching the yield or unstable collapse point (stage 2) characterized by a sharp load loss on the stress strain-curve up to a plateau or softening region in the case of G-Sil and G-Ep foam, respectively (stage 3). In stage 3, the compression stress was almost constant with strain for higher densities of G-Sil foams (i.e. for density values of 0.50 and 0.70 g/cm^3) as the cells deformed plastically; in those cases, after the yield stress was reached, the specimen continued to carry 3 MPa of stress up to relatively large strains, i.e. 25% of axial deformation. On the contrary, G-Ep foams showed a softening behaviour in stage 3 up to lower ultimate strains compared to G-Sil foams. The recorded discrepancy was probably due to the heterogeneous microstructure [32] of G-Ep matrix which was not able to accommodate the increased local deformation associated with the progressive collapse mechanism

of the cells. A further region of rapidly increasing load (densification region, stage 4) was recorded only in the case of higher density G-Sil foams.

The compressive strength of tested foamed materials was calculated from the maximum load applied to the specimens (corresponding to the yield or unstable collapse point - stage 2) while the Young's modulus under compression was derived from the slope of the initial linear region of the stress-strain diagram. The average values of compressive strength and Young's modulus (computed from measurements on three samples) are shown in Fig. 9a and Fig. 9b for G-Sil (blue symbols) and G-Ep (red symbols) foamed materials as a function of the relative density ρ^*/ρ_s, i.e. the ratio between the actual apparent density of the foam, ρ^*, and the density of the fully dense neat G-Sil and G-Ep materials, ρ_s, equal to 1.34 and 1.42 g/cm^3, respectively. For both foam material types, the overall results showed that the foaming process was able to produce satisfactory mechanical performances in reference to similar materials [20,22,30]. In particular, considering that average compressive strengths of fully dense neat G-Sil and G-Ep materials was 65 and 41 MPa, respectively [33], the corresponding compressive strengths of foamed samples varied between 11 and 0.67 MPa in the density range of 0.25–0.86 g/cm^3 (corresponding to 0.19 and 0.60 of relative density, respectively). As general tendency, G-Sil foamed material developed higher compressive strengths than G-Ep foam type in the density range of 0.45–0.70 g/cm^3
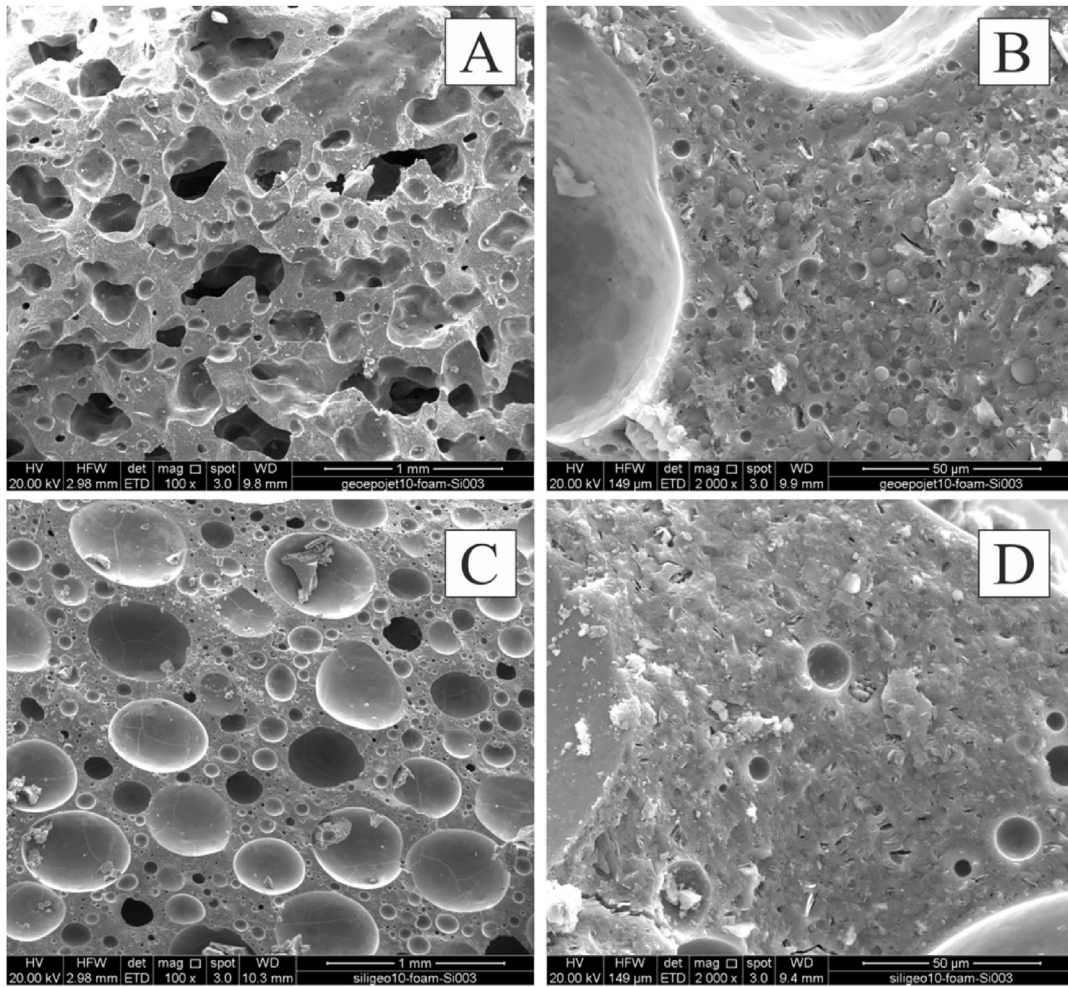
Fig. 3. SEM images at 100 (A, C) and 2000 (B, D) magnification of G-Ep03 (A, B) and G-Sil03 (C, D). In B and D, images of the wall between large pores are shown.
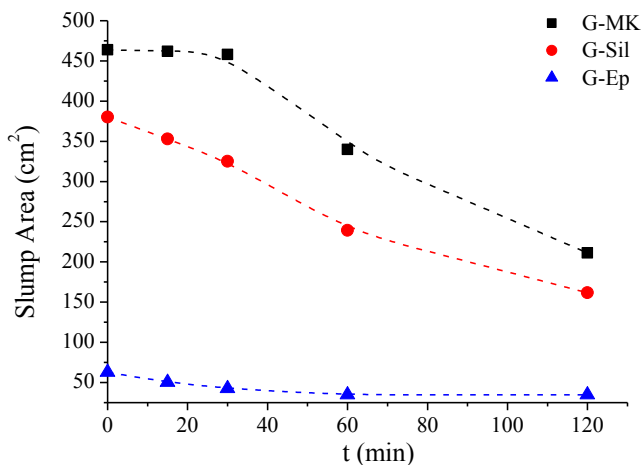

Fig. 4. Variation of slump area with time for G-MK (black squares), G-Sil (red circles) and G-Ep (blue triangles) slurries. Lines are a guide for the eyes. (For interpretation of the references to colour in this figure legend, the reader is referred to the web version of this article.)

$(0.34-0.52 \; \rho^*/\rho_s)$. The greatest difference was estimated in correspondence of a density value 0.70 g/cm^3 and was equal to 47%. Below the density threshold of 0.45 g/cm^3 (corresponding to a relative density between 0.35 and 0.40), this tendency was reversed in favour of G-Ep foams which exhibited, for instance, a compressive strength 40% greater than G-Sil foam in the case of 0.30 g/cm^3 of density (1.62 vs 1.15 MPa, respectively). This behaviour can be correlated to the deformation response of the two different cellular materials which is strongly influenced by corresponding value of relative density. At higher densities, the mechanical performance of the foamed material under compression typically approaches the compressive behaviour of the full dense material. Indeed, as reported in a previous study by the authors [27], in the full dense state, G-Sil material has averagely improved mechanical performances (either stiffness and strength) compared to G-Ep systems. On the other side, at low densities, compressive failure is typically caused by tensile failure of the bent cell walls of a given diameter. In this respect, full dense G-Sil was found to behave as a brittle material under failure [33] while G-Ep exhibited a moderate toughening mechanism (with regard to fracture) due to the presence of the discrete resin particles. Consequently, the tougher G-Ep was able to accommodate larger tensile strains under bending loads and, in turn, provide a more effective resistant mechanism to failure in compression at lower densities.

Stress-strain curves obtained by compressive tests allowed determining also the Young's modulus in compression of all samples (Fig. 8b). The elastic stiffness of the two foamed materials showed a similar dependency on the density values, resulting in Young's modulus values approximately ranging between 100 and
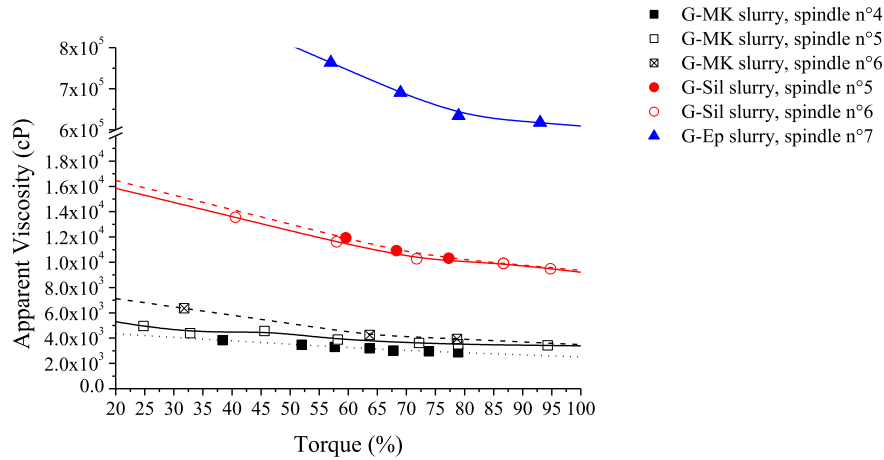
Fig. 5. Apparent viscosity of G-MK (squares), G-Sil (circles) and G-Ep (triangles) slurries as measured with the spindle indicated. Lines are a guide for the eyes.
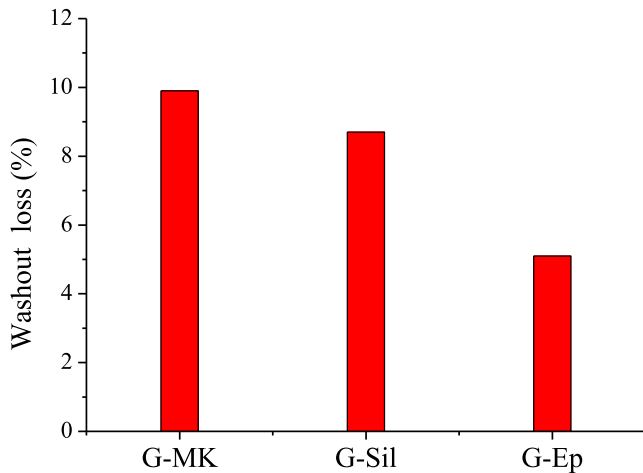

Fig. 6. Washout loss values for G-MK, G-Sil, G-Ep as determined on their freshly prepared slurries.
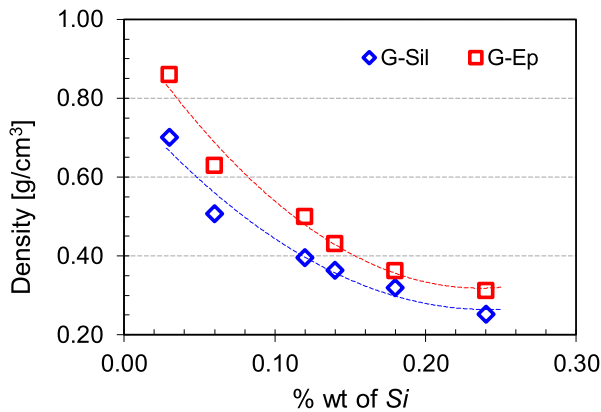

Fig. 7. Average apparent densities (over three samples) of G-Sil (blue symbols) and G-Ep (red symbols) foamed materials as a function of the foaming agent content (wt% of Si powder). (For interpretation of the references to colour in this figure legend, the reader is referred to the web version of this article.)

1400 MPa in the density interval of 0.25–0.86 g/cm³ (corresponding to 0.19 and 0.60 of relative density, respectively). Moreover, the overall trend of the results as a function of material

density, resulted very similar to the one observed for the compressive strength, i.e. with an inversion point in correspondence of a material density of approximately 0.45 g/cm³ (corresponding to a relative density between 0.35 and 0.40). In particular, for densities below 0.45 g/cm³, the Young's modulus of the foams is largely controlled by the volume fraction of large coalesced voids. In the case of G-Sil foam, brittle micro-cracking of bent coalesced voids may act as an additional contribution to deformation within the foam matrix, decreasing the initial stiffness. For densities above 0.45 g/cm³, the volume fraction of large coalesced voids is small and the Young's modulus of the G-Sil foam is controlled by the stiffer matrix compared with G-Ep one.

It's worth noting that within the density range 0.20–0.45 g/cm³ both foamed materials exhibited interesting compression properties, especially with reference to that density interval which represents an important range for technological applications of lightweight materials [23].

In terms of analytical interpretation of the results, we refer to the classical relationships between the strength (eq. (2)) or Young's modulus (eq. (3)) of a cellular material and its relative density proposed by Gibson-Ashby [54]:

$$\frac{\sigma_c^*}{\sigma_c^s} = C_1 \left(\frac{\rho^*}{\rho_s} \right)^m \tag{2}$$

$$\frac{E_c^*}{E_c^s} = C_2 \left(\frac{\rho^*}{\rho_s} \right)^n \tag{3}$$

where σ_c^*, E_c^* and ρ^* are the compressive or yield strength, the Young's modulus (in compression) and the relative density of the foam material, respectively; σ_c, E_c and ρ_s are the corresponding properties referred to the fully dense solid of which the foam is made or, in an equivalent manner, the properties of the solid cell wall material; C_1, C_2 are dimensionless constants and the exponents m, n depend on the cell morphology and can be established both by experiment and by numerical computation. These relationships can be successfully used to model the mechanical properties of most foams, whether open or closed cell, with a bending-dominated deformation behaviour. Dotted lines in Fig. 9 a,b represent the best fit of equations (2) and (3), the parameters of which are reported in Table 3.

As discussed in this section, the G-Sil and G-Ep foams behave as a linear elastic material up to the elastic limit under compression, at which point the cell edges failure takes place. The variations of
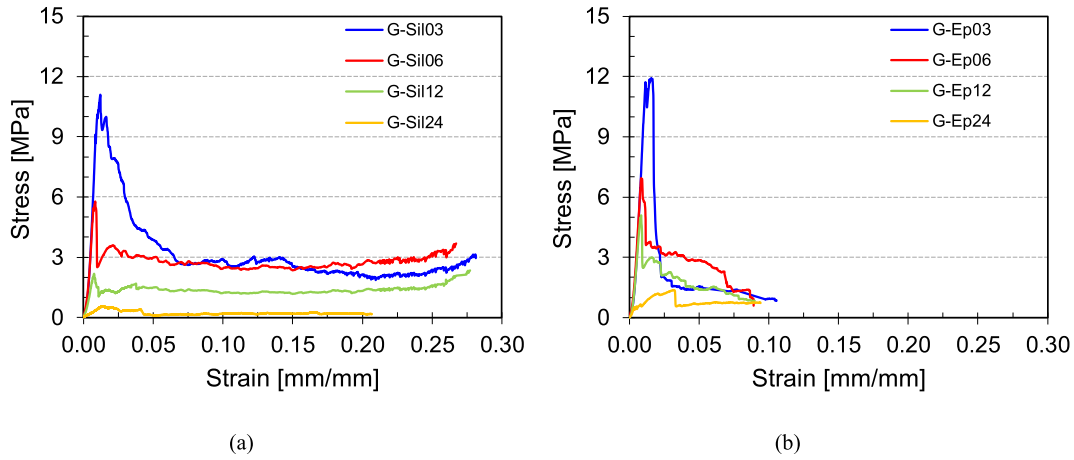
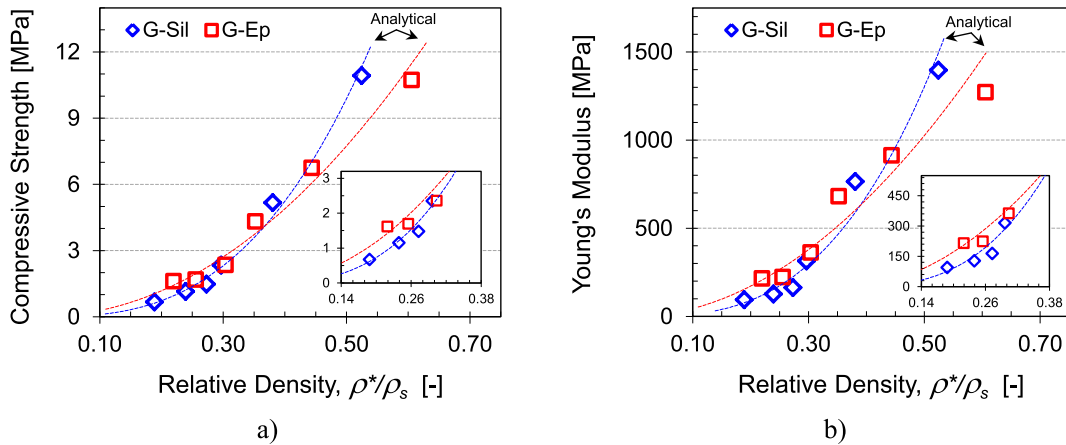Fig. 8. Stress-strain curves in compression of G-Sil (a) and G-Ep (b) samples.

Fig. 9. Average (over three samples) compressive strengths (a) and Young's modulus (b) for G-Sil (blue symbols) and G-Ep (red symbols) foamed materials as a function of the relative density. (For interpretation of the references to colour in this figure legend, the reader is referred to the web version of this article.)

Table 3
Parameters of data fitting reported in Fig. 9 a,b (dotted lines) according to equations (2) and (3).

	Compressive Strength		Young's modulus	
G-Ep-foam	C_1 [-]	0.79	C_2 [-]	1.52
	m [−]	2.05	n [−]	1.95
	σ_c^s [MPa] [27]	40.8	E_c^s [MPa] [27]	2600
G-Sil-Foam	C_1 [-]	1.15	C_2 [-]	2.35
	m [−]	2.85	n [−]	2.90
	σ_c^s [MPa] [27]	62.0	E_c^s [MPa] [27]	4160

Table 4
Density and $\lambda_{10,\,dry}$ of three different specimens of G-Ep12 and G-Sil12.

Sample	Density (kg/m^3)	$\lambda_{10,\,dry}$ (W/mK)
G-Ep12_1	480.1	0.101 ± 0.002
G-Ep12_2	500.5	0.103 ± 0.002
G-Ep12_3	523.6	0.105 ± 0.002
G-Sil12_1	396.2	0.101 ± 0.002
G-Sil12_2	395.5	0.105 ± 0.002
G-Sil12_3	398.0	0.103 ± 0.002

Young's modulus with the relative density follows equation (3) with the exponent n equal to 2 (G-Ep) or 3 (G-Sil), in agreement with previous results dealing with inorganic (cementitious) foams [55]; the different values of the exponent, n, between the two foamed materials can be related to the elastic properties of the corresponding fully dense solid ones.

A similar analysis can be conducted for the variation of the compressive strength with the relative density (equation (2)). The exponents m obtained from the best fit of the experimental data resulted higher that the ones suggested by Gibson-Ashby [54] (i.e. m = 3/2) probably due to several reasons. Primarily, the possibility of having mixed closed and open cells along with the presence of pores in most of the cell walls may have affected the failure

initiation under compression deformation. Secondly, the hybrid nature of the foams' microstructure may act as positive stabilization for the collapse limit especially at higher densities, for which the contribution of axial and shear stresses in the cell wall is dominant.

3.4. Thermal conductivity

Thermal conductivity tests were carried out on G-Sil12 and G-Ep12 samples. Table 4 shows the values of the volumetric density (kg/m^3) for each examined specimens and the corresponding $\lambda_{10,dry}$ values.

In both cases, the values of thermal conductivity are in the range 0.101−0.105 W/mK. Fig. 10 shows the relation between the
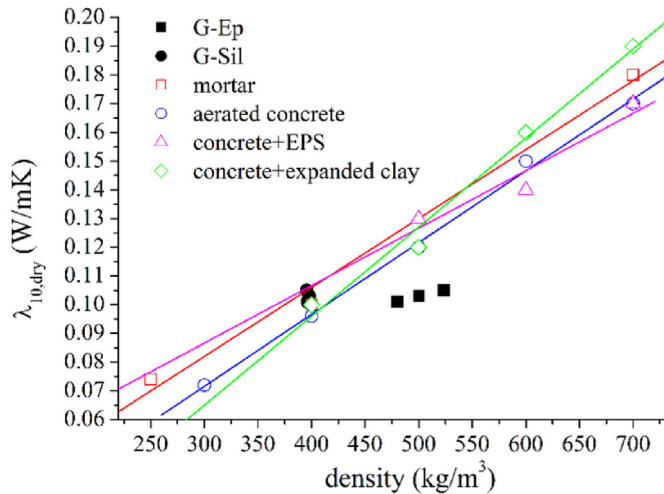
Fig. 10. Relation between $\lambda_{10,\text{ dry}}$ and density for G-Ep12 (black square); G-Sil12 (black circle); masonry mortars, Table. A12 of ref. [56] (red square); autoclaved aerated concrete, Table A10 of ref. [56] (blue circle); concrete with polystyrene aggregates, Table A5 of ref. [56] (magenta triangle); concrete with expanded clay aggregates, Table A6 of ref. [56] (green rhombus). All the straight lines represent P = 50% of the data. (For interpretation of the references to colour in this figure legend, the reader is referred to the web version of this article.)

experimental thermal conductivity and the measured density for G-Ep12 and G-Sil12 specimens. These results are compared with the values reported in Tables A of EN 12664 [56] for some representative lightweight materials used for masonry products. Each line refers to 50% fractiles for each category of materials. As far as G-Sil12, the results obtained are in the same range with those found for reference materials with the same density, while in the case of G-Ep12 the conductivity values obtained are far lower than 50% of the values reported in the reference materials with the same density thus indicating better insulating properties.

3.4.1. Flame tests

In order to obtain information on the combustion behaviour of the investigated materials under ventilated conditions, fire resistance tests were performed on G-Ep18 and G-Sil12 (i.e. samples showing similar apparent density values, see Table 2). The optical images of these samples before and after the cone calorimeter test are reported in Fig. 11.

The cone calorimeter showed that these specimens did not ignite, burn or release appreciable smoke even after extended heat flux exposure. Moreover, the heat release rate (HRR), that represents the contribution in terms of heat released by the material in case of fire, was minimal and also the CO, CO_2 and the produced fumes were of a negligible amount. In particular, G-Sil12 sample showed HRR and THR values (see Table 5), CO and CO_2 production (see Fig. 12) lower than G-Ep18 specimen.

Therefore, the foamed organic-inorganic materials described in the present paper can be considered as not-flammable, with a not significant production of toxic fumes and smokes. Thus they can efficiently replace the neat geopolymers in all the applications where exposure to flames and lightness are desired.

Table 5 summarizes the main outcomes of cone calorimeter tests conducted on the investigated foamed specimens.
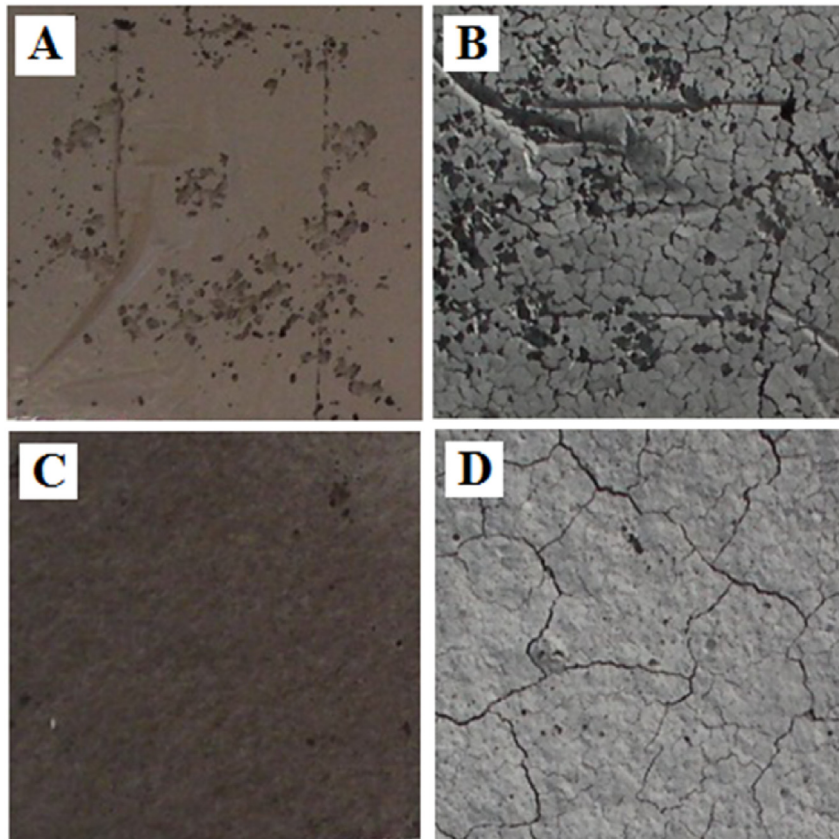

Fig. 11. Images of G-Ep18 (**A, B**) and G-Sil12 (**C, D**) before (**A, C**) and after (**B, D**) the cone calorimeter test.

Table 5
Flame tests results of G-Ep18 and G-Sil12, HRR = heat release rate, THR = total heat release.

Samples	HRR (peak) (kW/m^2)	HRR (60 s) (kW/m^2)	HRR (180 s) (kW/m^2)	THR (MJ/m^2)
G-Ep18	16.6	3.9	9.4	6.0
G-Sil12	7.4	2.1	1.4	1.1

4. Conclusions

Two different types of novel organic-inorganic geopolymer based foams were successfully manufactured by mixing metakaolin and an aqueous alkalisilicate solution with mixtures of dialkylsiloxane oligomers or organic resins precursors, respectively. The density of the obtained materials (ranging from 0.25 to 0.85 g/cm^3) was tailored by simply controlling the amounts of silicon
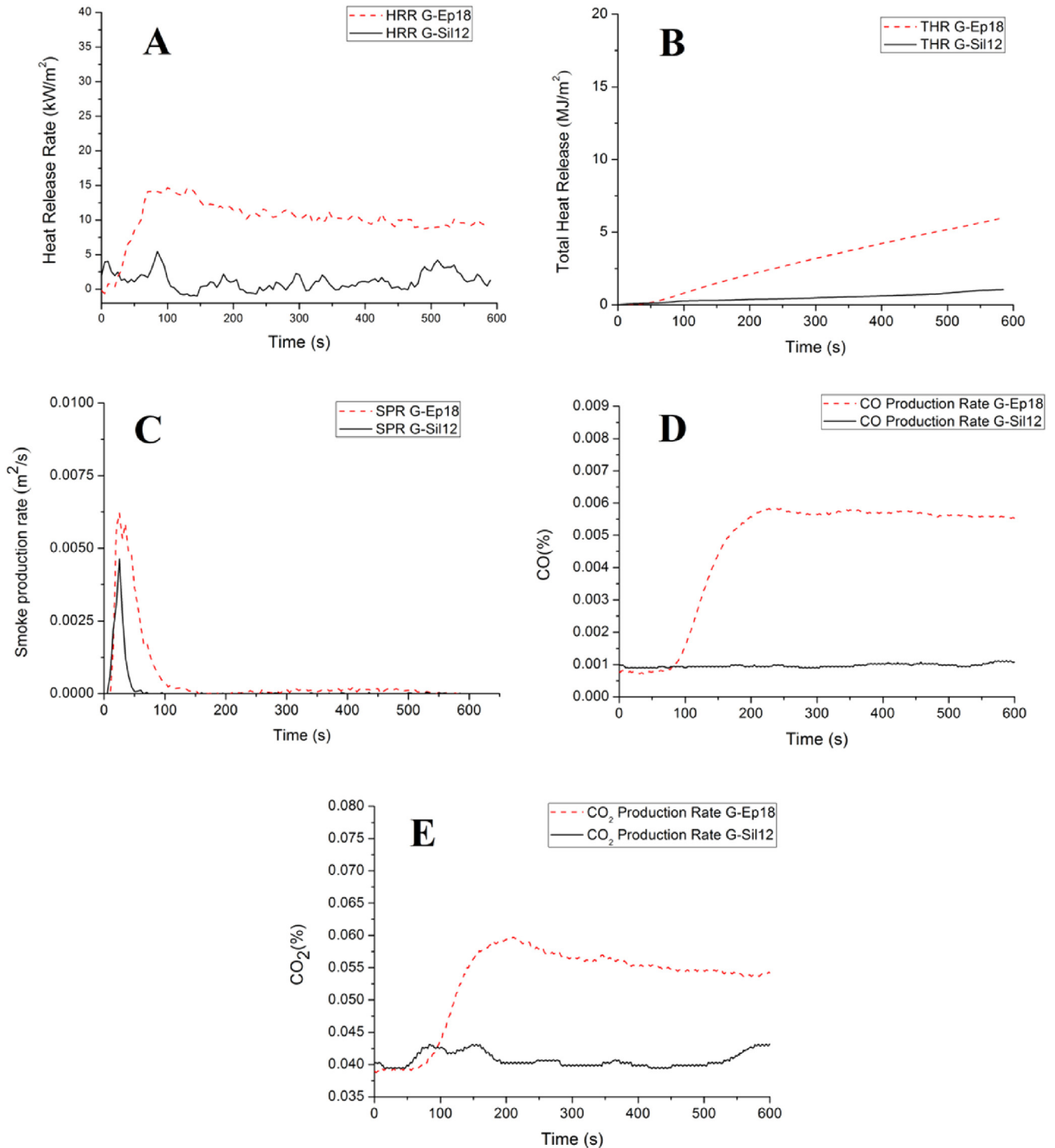

Fig. 12. Flame test results: (**A**) HRR-Heat Release Rate (kW/m^2) *vs* time (s); (**B**) THR-Total Heat Release (MJ/m^2) *vs* time; (**C**) SPR-Smoke production rate (m^2/s) *vs* time (s); (**D**) CO production (%) *vs* time (s); (**E**) CO$_2$ production (%) *vs* time (s) for G-Ep18 and G-Sil12.

powder added to the slurry as *in situ* foaming agent.

In both cases, the addition of the organic components or of the dialkylsiloxane oligomers, turned out in a significant change of the intrinsic viscosity of the geopolymeric slurry, thus allowing the obtainment of a homogeneous and very regular foaming process. In particular, in the case of the composite foamed materials obtained by adding the organic resin precursor to the geopolymeric slurry (G-Ep), the very high viscosity of the fresh mixture (in respect to neat geopolymeric one) has allowed obtaining a microstructure characterized by pore cells with a mean diameter up to 3 mm, in which, the dense spheres of epoxy resin forming the heterogeneous microstructure of the cell walls could have likely acted as physical hindrance for cell growth phase. At variance, in the case of G-Sil foams, the lower viscosity of the slurry allowed for a larger volume growth of the cells, which led to a decrease of the stability of the foam, causing, in turn, individual cells to coalesce thus producing larger voids.

These new porous materials, despite their cellular morphology, are still characterized by interesting mechanical properties. In particular, it is worth pointing out that, for both foamed materials, average compressive strengths up 5 MPa were recorded within the density range 0.2—0.5 g/cm^3, which represents an important range for technological applications of lightweight materials.

Moreover, within the same density range, both G-Sil and G-Ep foams exhibit good fire resistance and low thermal conductivity with λ values in the range 0.101—0.105 W/mK.

These properties are significantly better than those shown by neat geopolymer foams reported in the literature and comparable or even better than that of typical (not geopolymeric) inorganic foamed materials with similar densities and could be related to the hybrid nature of the materials used. In fact, as already shown in the case of their dense form, the synergistic effect of the organic and inorganic components of the developed materials has a beneficial effect on their properties.

For these reasons, it can be reasonably concluded that these new hybrid materials could represent a valid alternative to commonly used inorganic foams (e.g. Portland Cement foams) for insulation and lightweight applications, since they combine performance benefits and operational energy savings.

Acknowledgement

References

[1] Colangelo F, Messina F, Di Palma L, Cioffi R. Recycling of non-metallic automotive shredder residues and coal fly-ash in cold-bonded aggregates for sustainable concrete. Compos Part B Eng 2017;116:46—52.

[2] Colangelo F, Cioffi R. Mechanical properties and durability of mortar containing fine fraction of demolition wastes produced by selective demolition in South Italy. Compos Part B Eng 2017;115:43—50.

[3] Colangelo F, Cioffi R, Liguori B, Iucolano F. Recycled polyolefins waste as aggregates for lightweight concrete. Compos Part B Eng 2016;106:234—41.

[4] Colangelo F, Messina F, Cioffi R. Recycling of MSWI fly ash by means of cementitious double step cold bonding pelletization: technological assessment for the production of lightweight artificial aggregates. J Hazard Mater 2015;299:181—91.

[5] Singh N, Hui D, Singh R, Ahuja IPS, Feo L, Fraternali F. Recycling of plastic solid waste: a state of art review and future applications. Compos Part B Eng 2017;115:409—22.

[6] Qiao XC, Tyrer M, Poon CS, Cheeseman CR. Characterization of alkali-activated thermally treated incinerator bottom ash. Waste Manag 2008;28(10): 1955—62.

[7] Zhang LY. Production of bricks from waste materials - a review. Constr Build Mater 2013;47:643—55.

[8] Safiuddin M, Jumaat MZ, Salam MA, Islam MS, Hashim R. Utilization of solid wastes in construction materials. Int J Phys Sci 2010;13:1952—63.

[9] Rashad AM. Alkali-activated metakaolin: a short guide for civil engineer - an overview. Constr Build Mater 2013;41:751—65.

[10] Zhang HY, Kodur V, Qi SL, Cao L, Wu B. Development of metakaolin—fly ash based geopolymers for fire resistance applications. Constr Build Mater 2014;55:38—45.

[11] Provis JL, Bernal SA. Geopolymers and related Alkali-activated materials. Annu Rev Mat. Res 2014;44. 299—232.

[12] McLellan BC, Williams RP, Lay J, van Riessen A, Corder GD. Costs and carbon emissions for geopolymer pastes in comparison to ordinary portland cement. J Clean Prod 2011;19:1080—90.

[13] Davidovits J. Geopolymers: inorganic polymeric new materials. J Therm Anal 1991;37:1633—56.

[14] Rowles M, O'Connor B. Chemical optimisation of the compressive strength of aluminosilicate geopolymers synthesised by sodium silicate activation of metakaolinite. J Mat. Chem 2003;13:1161—5.

[15] Davidovits J. Geopolymer. Chemistry and applications. third ed. Saint Quentin, France: Institut Geopolymere; 2011.

[16] Habert G, Ouellet-Plamondon C. Recent update on the environmental impact of geopolymers. Rilem Tech Lett 2016;1:17—23.

[17] Duxson P, Provis JL, Lukey GC, Van Deventer JS. The role of inorganic polymer technology in the development of 'green concrete'. Cem Concr Res 2007;37(12):1590—7.

[18] Bell JL, Kriven WM. Preparation of ceramic foams from metakaolin-based geopolymer gels. In: Lin HT, Koumoto K, Kriven WM, Garcia E, Reimanis IE, Norton DP, editors. Developments in strategic materials: ceramic engineering and science proceedings; 2009. p. 97—111. 29(10).

[19] Prud'homme E, Michaud P, Joussein E, Peyratout C, Smith A, Rossignol S. In situ inorganic foams prepared from various clays at low temperature. Appl Clay Sci 2011;51:15—22.

[20] Medri V, Ruffini A. Alkali-bonded SiC based foams. J Eur.Ceram Soc 2011;32: 1907—13.

[21] Medri V, Papa E, Dedecek J, Jirglova H, Benito P, Vaccari A, et al. Effect of metallic Si addition on polymerization degree of in situ foamed alkali-aluminosilicates. Ceram Int 2013;39(7):7657—68.

[22] Verdolotti L, Liguori B, Capasso I, Errico A, Caputo D, Lavorgna M, et al. Synergistic effect of vegetable protein and silicon addition on geopolymeric foams properties. J Mat. Sci 2015;50:2459.

[23] Studart R, Gonzenbach UT, Tervoort E, Gauckler LJ. Processing routes to macroporous ceramics: a review. J Am Ceram Soc 2006;89:1771—89.

[24] Bourret J, Prud'homme E, Rossignol S, Smith DS. Thermal conductivity of geomaterial foams based on silica fume. J Mat. Sci 2012;47:391—6.

[25] Prud'homme E, Michauda P, Joussein E, Peyratout C, Smith A, Arii-Clacens S, et al. Silica fume as porogent agent in geo-materials at low temperature. J Eur Ceram Soc 2010;30:1641—8.

[26] Henon J, Alzina A, Absi J, Smith DS, Rossignol S. Potassium geopolymer foams made with silica fume pore forming agent for thermal insulation. J Porous Mater 2013;20:37—46.

[27] Feng J, Zhang R, Gong L, Li Y, Cao W, Chenget X. Development of porous fly ash-based geopolymer with low thermal conductivity. Mater Des 2015;65: 529—33.

[28] Abdollahnejad Z, Pacheco-Torgal F, Félix T, Tahri W, Barroso Aguiar J. Mix design, properties and cost analysis of fly ash-based geopolymer foam. Constr Build Mater 2015;80:18—30.

[29] Hlaváček P, Šmilauer V, Škvára F, Kopecký L, Šulc R. Inorganic foams made from alkali-activated fly ash: mechanical, chemicaland physical properties. J Eur Ceram Soc 2015;35:703—9.

[30] Zhang Z, Provis JL, Reid A, Wang H. Mechanical, thermal insulation, thermal resistance and acoustic absorption properties of geopolymer foam concrete. Cem Concr Compos 2015;62:97—105.

[31] Ferone C, Roviello G, Colangelo F, Cioffi R, Tarallo O. Novel hybrid organic-geopolymer materials. Appl Clay Sci 2013;73:42—50.

[32] Roviello G, Ricciotti L, Ferone C, Colangelo F, Cioffi R, Tarallo O. Synthesis and characterization of novel epoxy geopolymer hybrid composites. Materials 2013;6:3943—62.

[33] Roviello G, Menna C, Tarallo O, Ricciotti L, Ferone C, Colangelo F, et al. Preparation, structure and properties of hybrid materials based on geopolymers and polysiloxanes. Mater Des 2015;87:82—94.

[34] Colangelo F, Roviello G, Ricciotti L, Ferone C, Cioffi R. Preparation and characterization of new geopolymer-epoxy resin hybrid mortars. Materials 2013;6:2989—3006.

[35] Ferone C, Colangelo F, Roviello G, Asprone D, Menna C, Balsamo A, et al. Application-oriented chemical optimization of a metakaolin based geopolymer. Materials 2013;6:1920—39.

[36] Gottardi S, Toccoli T, Iannotta S, Bettotti P, Cassinese A, Barra M, et al. Optimizing picene molecular assembling by supersonic molecular beam deposition. J Phys Chem C 2012;116:24503—11.

[37] Menna C, Asprone D, Forni D, Roviello G, Ricciotti L, Ferone C, et al. Tensile behaviour of geopolymer-based materials under medium and high strain rates. EPJ Web Conf 2015;94. Article number 01034.

[38] Roviello G, Ricciotti L, Tarallo O, Ferone C, Colangelo F, Roviello V, et al.

Innovative fly ash geopolymer-epoxy composites: preparation, microstructure and mechanical properties. Materials 2016;9(6):461–75.

[39] Roviello G, Ricciotti L, Ferone C, Colangelo F, Tarallo O. Fire resistant melamine based organic-geopolymer hybrid composites. Cem Concr Compos 2015;59: 89–99.

[40] Ricciotti L, Borbone F, Carella A, Centore R, Roviello A, Barra M, et al. Synthesis of highly regioregular poly[3-(4-alkoxyphenyl)-thiophene]s by oxidative catalysis using copper complexes. J Polym Sci Part A Polym Chem 2013;51: 4351–60.

[41] Ricciotti L, Roviello G, Tarallo O, Borbone F, Ferone C, Colangelo F, et al. Synthesis and characterizations of melamine-based epoxy resins. Int J Mol Sci 2013;14:18200–14.

[42] Strini A, Roviello G, Ricciotti L, Ferone C, Messina F, Schiavi L, et al. TiO2-Based photocatalytic geopolymers for nitric oxide degradation. Materials 2016;9(7): 513–25.

[43] www.mapei.com/public/COM/products/367_epojet_gb.pdf.

[44] Matlab release R2015a - The MathWorks, Inc.

[45] Kantro DL. Influence of water-reducing admixtures on properties of cement paste—a miniature slump test. Cem Concr aggregates 1980;2(2):95–102.

[46] Collins F, Sanjayan JG. Early age strength and workability of slag pastes activated by NaOH and Na2CO3. Cem Concr Res 1998;28(5):655–64.

[47] Bouvet A, Ghorbel E, Bennacer R. The mini-conical slump flow test: analysis and numerical study. Cem Concr Res 2010;40(10):1517–23.

[48] Dubey R, Kumar P. An experimental study for optimization of high range water reducing superplasticizer in self compacting concrete. Front Struct Civ Eng 2013;7(1):62–71. 2013.

[49] Messina F, Ferone C, Colangelo F, Cioffi R. Low temperature alkaline activation of weathered fly ash: influence of mineral admixtures on early age performance. Constr Build Mater 2015;86:169–77.

[50] Lachemi M, Hossain KMA, Lambros V, Nkinamubanzi PC, Bouzoubaa N. Performance of new viscosity modifying admixtures in enhancing the rheological properties of cement paste. Cem Concr Res 2004;34(2):185–93.

[51] Talò M, Krause B, Pionteck J, Lanzara G, Lacarbonara W. An updated micromechanical model based on morphological characterization of carbon nanotube nanocomposites. Compos Part B Eng 2017;115:70–8.

[52] Khezrzadeh H. A statistical micromechanical multiscale method for determination of the mechanical properties of composites with periodic microstructure. Compos Part B Eng 2017;115:138–43.

[53] Fantilli AP, Frigo B, Chiaia B. Comparing multi-scale cracking mechanisms in man-made composites and natural materials. Compos Part B Eng 2017;115: 369–75.

[54] Gibson LJ, Ashby MF. Cellular solids: structure and properties. Cambridge university press; 1999.

[55] Tonyan TD, Gibson LJ. Structure and mechanics of cement foams. J Mater Sci 1992;27(23):6371–8.

[56] European Committee for Standardization (CEN). EN 12664. Thermal performance of building materials and products - Determination of thermal resistance by means of guarded hot plate and heat flow meter methods - Dry and moist products of medium and low thermal resistance. Tables A. Date of Availability 2001-01-24. 2001.